https://doi.org/10.20965/jrm.2020.p0994

Paper:

Flowrate Measurement in a Pipe Using Kalman-Filtering Laminar Flowmeter

Kazushi Sanada

Faculty of Engineering, Yokohama National University
79-5 Tokiwadai, Hodogaya, Yokohama, Kanagawa 240-8501, Japan
E-mail: sanada-kazushi-sn@ynu.ac.jp

[Received April 1, 2020; accepted June 30, 2020]

A laminar flowmeter that estimates the unsteady flowrate in a pipe using a Kalman filter is proposed. The laminar flowmeter has 32 narrow pipes. Kalman filtering is applied to one of the narrow pipes to estimate its flowrate. Three pressure sensors are connected to the narrow pipe. Upstream and downstream pressure signals are applied to a model of pipeline dynamics. The midpoint pressure is calculated and compared with the measured value. The error signal is fed back to the model. According to the principle of the Kalman filter, the estimated flowrate converges to the real flowrate. The Kalman-filtering estimation is conducted in a real-time computing system. In this study, the steady flowrate in a pipe is estimated and calibrated with measured data. The proposed Kalman-filtering-based laminar flowmeter demonstrates very promising performance.

Keywords: flowrate, measurement, incompressible fluid flow, laminar flowmeter, Kalman filter

1. Introduction

In recent years, hybrid excavators have gained attention in research field. Hybrid systems use an accumulator, battery, or super-capacitor for storing energy and recycling the stored energy for other drives [1–7]. The fluid power transmitted by a pipe is determined using pressure and flowrate. In a hybrid system, pressure can be easily detected using a commercial pressure sensor. In contrast, a flowrate sensor is not suitable for practical use, especially for unsteady flowrate measurement. However, the fluid power in a pipe can be detected using a flowrate sensor. This enables a more sophisticated control to store and recycle energy in hybrid systems.

The measurement of unsteady flowrate has been an important research topic. Most commercial flowmeters are suitable for the measurement of steady flowrate in a pipe. A few turbine-type and gear-type flowmeters can measure unsteady flowrate under limited conditions. There is a pressure drop across these flowmeters to some degree. Thus, an indirect measurement of unsteady flowrate using pipeline dynamics has been investigated to avoid pressure loss. A pipeline wave propagation model was used for the measurement of unsteady flowrate [8]. Zhao proposed a real-time measurement technique using a transfer function corresponding to pipeline dynamics [9].

The Kalman filter has been employed for flowrate measurement [10–17]. During the measurement of the flowrate in a pipe, the flowrate signal contains sensor noise. The Kalman filter theory has an advantage that the sum of squares of the estimation error is minimized under the assumption of linearity of the state equation of the target plant [18].

Previous studies have proposed estimation techniques for the flowrate in a pipe using a Kalman filter [19–24]. The Kalman filter uses the pipeline-dynamics model, which is an optimized finite-element model of pipeline dynamics [25]. Three pressure sensors are connected to a target pipe. Upstream and downstream pressure signals are applied to the pipeline-dynamics model, and the midpoint pressure is calculated by the model. The estimated midpoint pressure is compared with the measured value. The error signal is fed back to the pipeline-dynamics model so that the pressure and flowrate are estimated by the pipeline-dynamics model. According to the Kalman filter theory, the sum of squares of the estimation error is minimized under the assumption of linearity of pipeline dynamics of the target pipe.

Previous studies assumed a laminar flow condition in the target pipe [19–24]. This paper proposes a Kalman-filter-based laminar flowmeter that covers not only the laminar flow region but also the transient and turbulent flow regions. Several narrow pipes are bundled to build the laminar flowmeter. One of the narrow pipes is the target of flowrate measurement with the Kalman-filter. The measured data are presented herein.

The rest of this paper is organized as follows. In Section 2, the main symbols are defined. The Kalman filter theory is briefly introduced in Section 3. The laminar flowmeter is described in Section 4. The measured data are presented in Section 5. The results of this study are summarized in Section 6.

2. Nomenclature

A	cross-sectional area of the pipe
$\boldsymbol{A}_p$	system matrix of the pipeline model
$\boldsymbol{A}_{pd}$	discrete-time system matrix
$\boldsymbol{A}_{p0}$	system matrix
$\boldsymbol{B}$	coefficient matrix
$\boldsymbol{B}_p$	input vector
$\boldsymbol{B}_{pd}$	discrete-time input vector
c	wave propagation speed
$\boldsymbol{c}_p$	output vector for midpoint pressure
$\boldsymbol{c}_f$	output vector for flowrate
$\boldsymbol{E}$	coefficient matrix
$\boldsymbol{F}$	coefficient matrix
$\boldsymbol{g}$	Kalman filter gain
k	index number of sampling
L_1	distance between pressure sensors
L_2	distance between pressure sensors
N	the number of pressure variable
$\boldsymbol{P}$	a solution of the algebraic Riccati equation
p	pressure
$\boldsymbol{p}$	pressure vector
p_{down}	downstream pressure
p_f	pressure loss per unit length of pipe
p_{mid}	midpoint pressure
$\hat{p}_{mid}$	estimated midpoint pressure
p_{up}	upstream pressure
$\boldsymbol{p}_f$	pressure loss vector
$\overline{\boldsymbol{p}}$	input vector
Q	flow rate in the main pipe
q	flow rate in the narrow pipe
q_{down}	flow rate at downstream
q_{up}	flow rate at upstream
$\boldsymbol{q}$	flow rate vector
R	inner radius of the narrow pipe
Re	Reynolds number
t	time
u	dummy variable
$\boldsymbol{v}$	system noise vector
W	weighting function
w	measurement noise
x	distance along the pipe
$\boldsymbol{x}$	state variable vector of the plant
$\hat{\boldsymbol{x}}$	posteriori estimate
$\hat{\boldsymbol{x}}^-$	priori estimate
z^{-1}	delay operator
ρ	density of the fluid
ν	kinematic viscosity of the fluid
$\boldsymbol{\sigma}_v$	covariance vector of the system noise
σ_w	covariance of the measurement noise

3. Kalman Filter System for Flowrate Estimation

3.1. Model of Pipeline Dynamics

The Kalman filter algorithm uses time-domain signals containing noise and calculates the estimated signals of unknown variables. The estimation is periodically updated using a model of plant dynamics and the measurements of the plant. As a model of the plant dynamics, a model of pipeline dynamics is used in the Kalman filter for flowrate estimation.

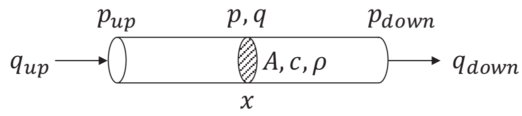

Fig. 1. Circular and uniform pipeline.

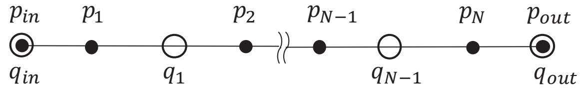

Fig. 2. Interlacing grid system.

A previous study proposed an optimized finite-element model of pipeline dynamics [25] in the form of a state-space equation. The coefficient matrices of the state-space representation are used in the Kalman filter algorithm. The model is described briefly in this section.

The optimized finite-element model of pipeline dynamics is based on the equation of motion (Eq. (1)) and continuity equation (Eq. (2)) of a one-dimensional incompressible fluid flow in a circular and uniform pipe shown in **Fig. 1**.

$$\frac{\partial q}{\partial t} + \frac{A}{\rho}\frac{\partial p}{\partial x} + p_f(q) = 0, \quad (1)$$

$$\frac{\partial p}{\partial t} + \frac{\rho c^2}{A}\frac{\partial q}{\partial x} = 0. \quad (2)$$

The interlacing grid system shown in **Fig. 2** is applied, and thus, the finite-element approximation of the equation of motion and continuity equation yields:

$$\frac{d\boldsymbol{q}}{dt} + \frac{A}{\rho}\boldsymbol{B}\boldsymbol{p} + \frac{A}{\rho}\boldsymbol{F}\overline{\boldsymbol{p}} + \boldsymbol{p}_f(\boldsymbol{q}) = \boldsymbol{0}, \quad (3)$$

$$\frac{d\boldsymbol{p}}{dt} + \frac{\rho c^2}{A}\boldsymbol{E}\boldsymbol{q} = \boldsymbol{0}. \quad (4)$$

The vectors $\boldsymbol{q}$ and $\boldsymbol{p}$ represent the flowrate and pressure variables at each grid point, respectively.

$$\boldsymbol{q} = [q_{up}, q_1, \ldots, q_{N-1}, q_{down}]^{\mathrm{T}}, \quad (5)$$

$$\boldsymbol{p} = [p_1, p_2, \ldots, p_N]^{\mathrm{T}}. \quad (6)$$

The term $\overline{\boldsymbol{p}}$ represents the input vector of the pressure at both ends of the pipe.

$$\overline{\boldsymbol{p}} = [p_{up}, p_{down}]^{\mathrm{T}}. \quad (7)$$

The above equations are combined, and thus, the finite-element model is represented as

$$\frac{d\boldsymbol{x}}{dt} = \boldsymbol{A}_{p0}\boldsymbol{x} + \boldsymbol{B}_p\overline{\boldsymbol{p}} - \begin{bmatrix}\boldsymbol{p}_f \\ \boldsymbol{0}\end{bmatrix}, \quad (8)$$

where the state variable vector is given by

$$\boldsymbol{x} = \left[\boldsymbol{q}^{\mathrm{T}}, \boldsymbol{p}^{\mathrm{T}}\right]^{\mathrm{T}}, \quad (9)$$

and the coefficient matrices are given by

$$\boldsymbol{A}_{p0} = \begin{bmatrix} \boldsymbol{0} & -\dfrac{A}{\rho}\boldsymbol{B} \\ -\dfrac{\rho c^2}{A}\boldsymbol{E} & \boldsymbol{0} \end{bmatrix}, \quad \ldots \ldots \ldots \quad (10)$$

$$\boldsymbol{B}_p = \begin{bmatrix} -\dfrac{A}{\rho}\boldsymbol{F} \\ \boldsymbol{0} \end{bmatrix}. \quad \ldots \ldots \ldots \quad (11)$$

A previous study proposed the minimization of the error of the un-damped natural angular frequencies of a model with respect to the theoretical ones by tuning the grid spacing [25].

Steady laminar friction is represented as

$$p_f(q) = \frac{8\nu}{R^2}q. \quad \ldots \ldots \ldots \quad (12)$$

Frequency-dependent laminar friction can be used as follows [26]:

$$p_f(q) = \frac{8\nu}{R^2}q + \frac{4\nu}{R^2}\int_0^t W(t-u)\frac{\partial q}{\partial t}(u)\,du. \quad . \quad (13)$$

The intermediate variables for representing the weighting function of the frequency-dependent friction are introduced [27], and thus, the representation of the optimized finite-element model becomes

$$\frac{d\boldsymbol{x}}{dt} = \boldsymbol{A}_p\boldsymbol{x} + \boldsymbol{B}_p\overline{\boldsymbol{p}}. \quad \ldots \ldots \ldots \quad (14)$$

The input vector $\overline{\boldsymbol{p}}$ includes the upstream and downstream pressures of the measurement section of the target pipe. The estimated pressure variable at the midpoint is obtained from the state variable vector as follows:

$$\hat{p}_{mid} = [\,\boldsymbol{0},\ 0\cdots1\cdots0\,]\begin{bmatrix}\boldsymbol{q}\\ \boldsymbol{p}\end{bmatrix} = \boldsymbol{c}_p\boldsymbol{x}. \quad \ldots \quad (15)$$

The vector $\boldsymbol{c}_p$ is an output vector as shown in Eq. (15). The estimated midpoint pressure $\hat{p}_{mid}$ is one of the variables of the pressure vector $\boldsymbol{p}$. The output vector $\boldsymbol{c}_p$ has the element "1" in the column corresponding to the midpoint pressure $\hat{p}_{mid}$ of the pressure vector $\boldsymbol{p}$.

3.2. Kalman Filter System

The optimized finite-element model is transformed into a discrete-time representation with system noise and sensor noise as follows:

$$\boldsymbol{x}(k+1) = \boldsymbol{A}_{pd}\boldsymbol{x}(k) + \boldsymbol{B}_{pd}\overline{\boldsymbol{p}}(k) + \boldsymbol{B}_{pd}\boldsymbol{v}(k), \quad . \quad (16)$$

$$\hat{p}_{mid}(k) = \boldsymbol{c}_p\boldsymbol{x}(k) + w(k). \quad \ldots \ldots \quad (17)$$

The system parameters $\boldsymbol{A}_{pd}$ and $\boldsymbol{B}_{pd}$ are obtained from the discretization of the coefficient matrices $\boldsymbol{A}_p$ and $\boldsymbol{B}_p$ of the optimized finite-element model of pipeline dynamics. The coefficient matrices $\boldsymbol{A}_p$ and $\boldsymbol{B}_p$ are the results of the finite-element approximation of the equation of motion, Eq. (1), and continuity equation, Eq. (2). The detailed description of the finite-element approximation is available elsewhere [25]. The identification of the coefficient matrices requires the following physical parameters: the cross-sectional area of the narrow pipe A, wave speed c, liquid density ρ, and kinematic viscosity of the fluid ν.

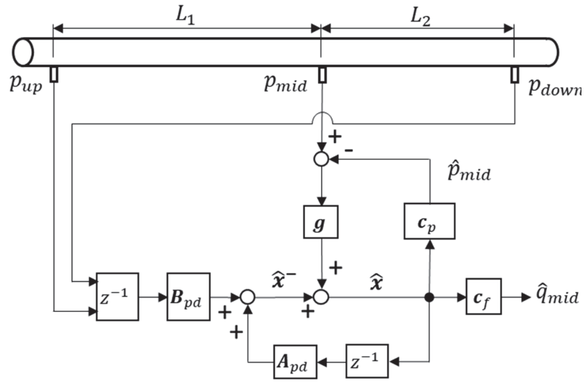

Fig. 3. Kalman filter for flowrate estimation.

The Kalman filter algorithm is performed via two-step estimation. The a priori estimate $\hat{\boldsymbol{x}}^-(k)$ and a posteriori estimate $\hat{\boldsymbol{x}}(k)$ are expressed as

$$\hat{\boldsymbol{x}}^-(k) = \boldsymbol{A}_{pd}\hat{\boldsymbol{x}}(k-1) + \boldsymbol{B}_{pd}\overline{\boldsymbol{p}}(k-1), \quad \ldots \quad (18)$$

$$\hat{\boldsymbol{x}}\ \ (k) = \hat{\boldsymbol{x}}^-(k) + \boldsymbol{g}(k)\left(p_{mid} - \boldsymbol{c}_p\hat{\boldsymbol{x}}(k)\right). \quad \ldots \quad (19)$$

The gain $\boldsymbol{g}$ is the Kalman filter gain. A steady-state Kalman filter uses a constant gain $\boldsymbol{g}$ as follows:

$$\boldsymbol{g} = \frac{\boldsymbol{P}\boldsymbol{c}_p^{\mathrm{T}}}{\boldsymbol{c}_p\boldsymbol{P}\boldsymbol{c}_p^{\mathrm{T}} + \sigma_w^2} \quad \ldots \ldots \ldots \quad (20)$$

The matrix $\boldsymbol{P}$ is obtained by solving the following algebraic Riccati equation as

$$\boldsymbol{P} = \boldsymbol{A}_{pd}\left[\boldsymbol{P} - \frac{\boldsymbol{P}\boldsymbol{c}\boldsymbol{c}^{\mathrm{T}}\boldsymbol{P}}{\boldsymbol{c}_p\boldsymbol{P}\boldsymbol{c}_p^{\mathrm{T}} + \sigma_w^2}\right]\boldsymbol{A}_{pd}^{\mathrm{T}} + \boldsymbol{\sigma}_v^2\boldsymbol{B}_{pd}\boldsymbol{B}_{pd}^{\mathrm{T}}. \quad (21)$$

The covariances of measurement noise and system noise, that is, σ_w^2 and $\boldsymbol{\sigma}_v^2$, respectively, are expressed as

$$\sigma_w^2 = E\left(w^2\right) = \left(1\times10^4\right)^2, \quad \ldots \ldots \quad (22)$$

$$\boldsymbol{\sigma}_v^2 = E\left(\boldsymbol{v}\boldsymbol{v}^{\mathrm{T}}\right) = \left(1\times10^4\right)^2 I_{2\times2}, \quad \ldots \quad (23)$$

where $E(\ )$ represents the expected value of the variable. The covariances were determined from the pressure sensor noise whose amplitude was 0.01 MPa ($= 1\times10^4$ Pa).

A block diagram of the Kalman filter is shown in **Fig. 3**. The upstream pressure p_{up} and downstream pressure p_{down} are measured and applied to the model of pipeline dynamics. The distance between the upstream and the midpoint pressure sensor and that between the midpoint and the downstream pressure sensor are represented by L_1 and L_2, respectively. The midpoint pressure $\hat{p}_{mid}$ is estimated and compared with the measured pressure p_{mid}. The error signal is multiplied by the gain $\boldsymbol{g}$ and fed back to the model. Under the assumption of linearity of the state equation, it is theoretically shown that the optimum filter is the Kalman filter in the sense that the sum of squares of the estimation error is minimized [18]. The estimated flowrate in the target narrow pipe $\hat{q}_{mid}$ is obtained by multiplying $\hat{\boldsymbol{x}}(k)$ by the output vector $\boldsymbol{c}_f$.

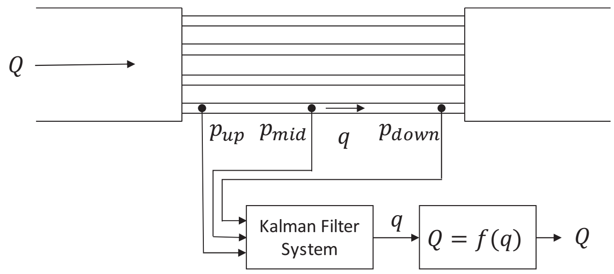

Fig. 4. Laminar flowmeter proposed in this paper.

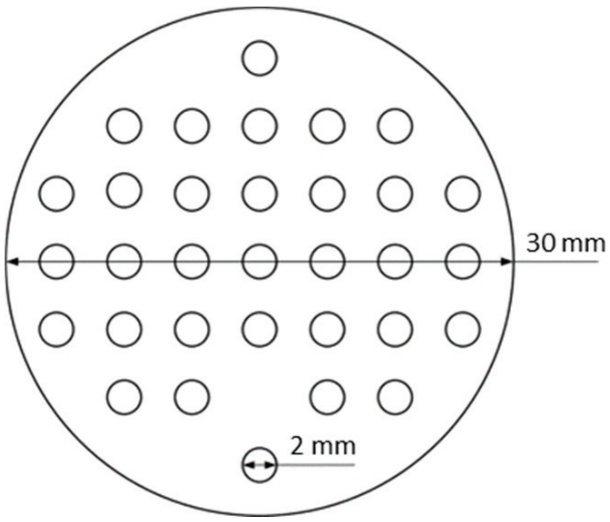

Fig. 5. Layout of the narrow pipes.

4. Laminar Flowmeter

The proposed laminar flowmeter is shown in **Fig. 4**. The cross section is presented in **Fig. 5**, which illustrates the layout of the narrow pipes of the laminar flowmeter. The main flow Q is divided among 32 narrow pipes. Each narrow pipe has an inner diameter of 1 mm and an outer diameter of 2 mm. Tap water is used as the working fluid. The laminar flowmeter is made of a stainless-steel pipe. Three pressure sensors are connected to one of the narrow pipes as shown in **Fig. 4**. The pressure sensors are AP-12S (Keyence) whose rated pressure is 100 kPa. The amplifier unit is AP-V80 (Keyence). The resolution is 0.1 kPa and the hysteresis is 0.5% of FS. The measured pressure signals are input to the Kalman filter to estimate the flowrate q in the target narrow pipe. The main flowrate Q is estimated from the relationship between the main flowrate and the flowrate of the narrow pipe.

5. Experimental Calibration

The experimental setup is shown in **Fig. 6**. Tap water is supplied to the laminar flowmeter. The flowrate of the tap water is adjusted with a water tap. For a precise calibration of the laminar flowmeter, a tank and load cell are set in the downstream to measure the main flowrate Q using the “catch-and-weigh” technique.

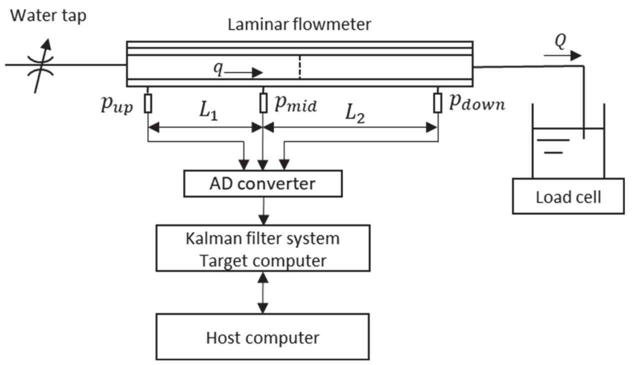

Fig. 6. Experimental setup.

Three pressure signals, p_{up}, p_{mid}, and p_{down}, are applied to the Kalman filter system through an analog-to-digital (AD) converter. The distances between the pressure sensors, L_1 and L_2, are 470 mm and 330 mm, respectively. These lengths are the same as those used in the “secondary source method” [28–30] to avoid a half-wave length condition.

It is assumed that the tap water has a kinematic viscosity of 1×10^{-6} m^2/s (1 cSt) and density of 1000 kg/m^3. Thus, when the flowrate of 5×10^{-5} m^3/s (3 L/min) is uniformly divided among the 32 narrow pipes having an inner diameter of 1 mm, the Reynolds number of each narrow pipe is 1990 and the pressure drop across each narrow pipe having a length of $L_1 + L_2$ is 51 kPa.

The Kalman filter system is built using MATLAB/Simulink. The block diagram is compiled and downloaded to a real-time computing system (sBOX II, TI, OMAP-L137 EVM, 372 MHz, 32 bit, floating point). The estimated flowrate and pressure signals are monitored by the host computer. The sampling period of the Kalman filter is 1 ms. The model of pipeline dynamics for the Kalman filter, that is, the optimized finite-element model has the number of elements N of 5 considering the frequency-dependent laminar friction model [31–33].

The main purpose of the experiments is the calibration of the proposed laminar flowmeter under a steady-state flow condition. A steady-state water flow was supplied to the laminar flowmeter by opening the water tap at a certain position. The flowrate was estimated by the Kalman filter system. The flowrate in the main pipe was measured using the “catch-and-weigh” technique for calibration. The measured flowrate data are plotted in **Fig. 7**. The horizontal axis is the flowrate q of the narrow pipe estimated by the Kalman filter system. The vertical axis is the main flowrate Q. When the estimated flowrate in the narrow pipe q is less than 0.18×10^{-5} m^3/s, the Reynolds number is less than 2300, indicating a laminar flow region. A main flow less than 3.5×10^{-5} m^3/s represents a laminar flow. In the laminar flow region of the narrow pipe, the main flowrate Q is represented by a linear function of the estimated flowrate q as follows:

$$Q = 30.0q. \qquad (24)$$

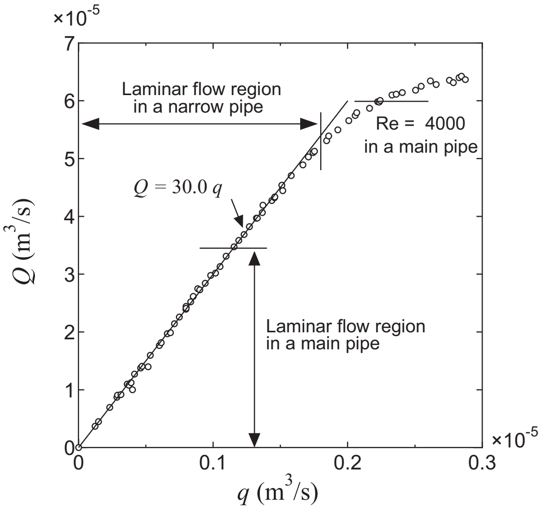

Fig. 7. Estimated flow rate in the narrow pipe q and the measured flow rate Q in the main pipe.

Based on this linear function, the main flowrate Q can be measured from the estimated flowrate q of the narrow pipe.

As shown in **Fig. 7**, within the laminar flow region of the narrow pipe, the flowrate q shows a linear relationship with the main flowrate Q. However, the coefficient 30 of Eq. (24) does not match the number of narrow pipes, 32. The reason is that the narrow pipe whose pressure is measured, that is, the bottom one, is located slightly away from the other narrow pipes as shown in **Fig. 5**. The pressure sensors are connected to the bottom narrow pipe. A small manifold block is used to connect the narrow pipe with the pressure sensor. Because of the manifold block, the target narrow pipe should be located away from the other narrow pipes. Due to the layout, the main flow is not uniformly divided among the 32 narrow pipes. A uniform layout is required for matching the coefficient with the number of narrow pipes.

A main flowrate Q less than 3.5×10^{-5} m^3/s indicates a laminar flow. When the main flowrate is 6×10^{-5} m^3/s, the Reynolds number of the main flow is 4000. This flow region is the transient region from laminar to turbulent flow. The laminar flow region in the narrow pipe covers not only the laminar flow region but also a part of the transient flow region of the main flow. The laminar flowmeter can estimate the main flowrate from the laminar to transient flow region.

6. Conclusions

A new laminar flowmeter was proposed and calibrated through experiments. The flowrate estimation using a Kalman filter algorithm was applied to a narrow pipe of the laminar flowmeter. The main flowrate was estimated through the relationship between flowrate of the narrow pipe and the main flowrate. The relationship covers not only the laminar flow region but also the transient flow region of the main flow. The coefficient of the relationship does not coincide with the number of narrow pipes. The relationship is obtained via experiments. It is necessary to explain the relationship from a theoretical point of view.

In the future, the proposed laminar flowmeter can be used to study unsteady flow measurement. The unsteady flow generated by using a solenoid valve will be measured using the laminar flowmeter.

Acknowledgements

The author would like to thank S. Hirano for his valuable contribution to this research. This study is supported by a Grant-in-Aid for Scientific Research (C) (JSPS KAKENHI Grant Number JP17K06226).

References:

[1] K. Sugimura and K. Suzuki, "Using Intermittently Operated Oil Hydraulic Pump Unit with Accumulator to Save Energy," Int. J. Automation Technol., Vol.6, No.4, pp. 426-433, 2012.

[2] P. Casoli, L. Riccò, F. Campanini, and A. Bedotti, "Hydraulic hybrid excavator–mathematical model validation and energy analysis," Energies, Vol.9, No.12, 1002, 2016.

[3] X. Lin, S. Pan, and D. Wang, "Dynamic simulation and optimal control strategy for a parallel hybrid hydraulic excavator," J. of Zhejiang University SCIENCE A, Vol.9, No.5, pp.624-632, 2008.

[4] T. Lin, Q. Wang, B. Hu, and W. Gong, "Research on the energy regeneration systems for hybrid hydraulic excavators," Automation in Construction, Vol.19, No.8, pp. 1016-1026, 2010.

[5] H. Kima, S. Yoob, S. Chob, and K. Yi, "Hybrid control algorithm for fuel consumption of a compound hybrid excavator," Automation in Construction, Vol.68, pp. 1-10, 2016.

[6] Y. Yua and K. Ahn, "Optimization of energy regeneration of hybrid hydraulic excavator boom system," Energy Conversion and Management, Vol.183, pp. 26-34, 2019.

[7] Q. Chena, T. Lina, H. Rena, and S. Fua, "Novel potential energy regeneration systems for hybrid hydraulic excavators," Mathematics and Computers in Simulation, Vol.163, pp. 130-145, 2019.

[8] N. Johnston, M. Pan, S. Kudzma, and P. Wang, "Use of Pipeline Wave Propagation Model for Measuring Unsteady Flow Rate," J. of Fluids Engineering, Vol.136, No.3, 031203, 2014.

[9] T. Zhao, K. Sanada, A. Kitagawa, and T. Takenaka, "Real Time Measurement for High Frequency Pulsating Flow Rate in a Pipe," Trans. of the ASME, J. of Dynamic Systems, Measurement, and Control, Vol.112, No.4, pp. 762-768, 1990.

[10] C. Shao, K. Xu, and Z. Shu, "Segmented Kalman filter based anti-strong transient impact method for vortex flowmeter," IEEE Trans. on Instrumentation and Measurement, Vol.66, Issue 1, pp. 93-103, 2017.

[11] X. Huang, S. Yue, H. Zhang, and B. Sun, "The prediction of energy-saving electromagnetic flowmeter based on Kalman filtering method," 2015 IEEE Int. Conf. on Applied Superconductivity and Electromagnetic Devices (ASEMD), pp. 262-263, 2015.

[12] M. Akresh, W. D. Walker, and L. Reindl, "Flow measurement using Kalman filter for smoothing vortex shedding frequency," Proc. of 2010 IEEE Instrumentation & Measurement Technology Conf., pp. 234-237, 2010.

[13] A. Venugopal, A. Agrawal, and S. V. Prabhu, "Review on vortex flowmeter–Designer perspective," Sensors and Actuators A, Vol.170, Issues 1-2, pp. 8-23, 2011.

[14] A. Dadashnialehi and B. Moshiri, "Online monitoring of transit-time ultrasonic flowmeters based on fusion of optical observation," Measurement, Vol.44, Issue 6, pp. 1028-1037, 2011.

[15] X. Huang and S. Yue "The Energy-Saving Strategy of Electromagnetic Flowmeters Based on Various Predicting Methods," IEEE Trans. on Applied Superconductivity, Vol.26, Issue 7, pp. 1-5, 2016.

[16] C. Shao, K. Xu, and Z. Shu, "Segmented Kalman filter based anti-strong transient impact method for vortex flowmeter," IEEE Trans. on Instrumentation and Measurement, Vol.66, Issue 1, pp. 93-103, 2017.

[17] X. Huang, S. Yue, H. Zhang, and B. Sun, "The prediction of energy-saving electromagnetic flowmeter based on Kalman filtering method," 2015 IEEE Int. Conf. on Applied Superconductivity and Electromagnetic Devices (ASEMD), pp. 262-263, 2015.

[18] S. Adachi and I. Maruta, "Fundamentals of Kalman Filter," Tokyo Denki University Press, 2017 (in Japanese).

[19] A. Ozawa, B. Gao, and K. Sanada, "Estimation of fluid transients in a pipe using Kalman filter based on optimized finite-element model," SICE Annual Conf. 2010, pp. 1652-1657, 2010.

[20] A. Ozawa and K. Sanada, "An indirect measurement method of transient pressure and flow rate in a pipe," Proc. of the 8th Int. Symp. on Fluid Power, Okinawa 2011, pp. 104-109, 2011.

[21] K. Sanada, "Using a Kalman filter to estimate unsteady flow," Int. J. Automation Technol., Vol.6, No.4, pp. 440-444, 2012.

[22] K. Sanada, "Simulation of Pipeline Dynamics Using an Optimized Finite Element Model," J. Robot. Mechatron., Vol.11, No.4, pp. 283-288, 1999.

[23] A. Ozawa and K. Sanada, "An indirect measurement method of transient pressure and flow rate in a pipe," Proc. of the 8th Int. Symp. on Fluid Power, Okinawa 2011, pp. 104-109, 2011.

[24] K. Sanada, "Using a Kalman filter to estimate unsteady flow," Int. J. Automation Technol., Vol.6, No.4, pp. 440-444, 2012.

[25] K. Sanada, C. W. Richards, D. K. Longmore, and D. N. Johnston, "A finite-element model of hydraulic pipelines using an optimized interlacing grid system," Proc. of Institution of Mech Engineers, Part I: J. of Systems and Control Engineering, Vol.207, No.4, pp. 213-222, 1993.

[26] W. Zielke, "Frequency-Dependent Friction in Transient Pipe Flow," J. of Basic Engineering, Vol.90, No.1, pp. 109-115, 1968.

[27] T. Kagawa, I. Lee, A. Kitagawa, and T. Takenaka, "High Speed and Accurate Computing Method of Frequency-Dependent Friction in Laminar Pipe Flow for Characteristics Method," Trans. of the Japan Society of Mechanical Engineers (JSME), Series B, Vol.49, No.447, pp. 2638-2644, 1983.

[28] D. N. Johnston and J. E. Drew, "Measurement of Positive Displacement Pump Flow Ripple and Impedance," Proc. of Institution for Mechanical Engineers, Part I, Vol.210, No.1, pp. 65-74, 1996.

[29] D. N. Johnston, "The Transmission Line Method for Modelling Laminar Flow of Liquid in Pipelines," Proc. of Institution for Mechanical Engineers, Part I, Vol.226, No.5, pp. 586-597, 2012.

[30] D. N. Johnston and K. A. Edge, "In Situ Measurement of the Wave speed and Bulk Modulus in Hydraulic Lines," Proc. of Institution for Mechanical Engineers, Part I, Vol.205, No.3, pp. 191-197, 1991.

[31] K. Sanada, "A study on order reduction of optimized finite-element model of pipeline dynamics," Int. J. of Fluid Power System (JFPS), Vol.8, No.1, pp. 18-23, 2015.

[32] K. Sanada, "Real-time implementation of Kalman filter for unsteady flow measurement in a pipe," Int. J. of Hydromechatronics, Vol.1, No.1, pp. 3-15, 2018.

[33] K. Sanada, "Condition for real-time measurement of power of unsteady fluid flow in a pipe by Kalman filter," Proc. of 11th Int. Fluid Power Conf., pp. 178-185, 2018.

Name:
Kazushi Sanada

Affiliation:
Professor, Yokohama National University

Address:
79-5 Tokiwadai, Hodogaya, Yokohama, Kanagawa 240-8501, Japan

Brief Biographical History:

1986- Research Assistant, Tokyo Institute of Technology
1998- Associate Professor, Yokohama National University
2004- Professor, Yokohama National University

Main Works:

• "Using a Kalman Filter to Estimate Unsteady Flow," Int. J. Automation Technol., Vol.6, No.4, pp. 440-444, 2012.

Membership in Academic Societies:

• The Japan Fluid Power System Society (JFPS)
• The Japan Society of Mechanical Engineers (JSME)
• The Society of Instrument and Control Engineers (SICE)